Synthesis and identification of the adducts of fullerenol-24 with some transition and rare earth metals

© V.V. Kuznetsov[3], N.A. Kulenova[1], B.K. Shaimardanova[1], M.A. Sadenova[1], L.V. Shushkevich[1], A.A. Blokhin[1,2], N.A. Charykov[1,2,3], A.A. Gurieva[2], V.P. German[2], V.A. Keskinov[1,2]

[1] Veritas Center, D. Serikbayev East Kazakhstan State Technical University, Ust-Kamenogorsk, Kazakhstan
[2] St. Petersburg State Technological Institute (Technical University), St. Petersburg, Russia,
[3] St. Petersburg State Electrotechnical University „LETI", St. Petersburg, Russia

E-mail: vv kuznetsov@inbox.ru

Received April 28, 2023
Revised September 5, 2023
Accepted October 30, 2023

The synthesis of fullerenol-24 ($C_{60}(OH)_{24}$) with some transition and rare earth metals — $C_{60}(ONa)_x(O_2M)_{(24-x)/2}$, $C_{60}(ONa)_x(O_3M)_{(24-x)/3}$, M = Co, Cu, Mn, Zn, Gd, Tb is described. Identification of adducts was carried out using the methods of elemental analysis, infrared and electron spectroscopy, complex thermal analysis, high-performance liquid chromatography and dynamic light scattering. The solubility of adducts in aqueous solutions in the natural temperature range has been studied. The use of these adducts as microfertilizers for spring barley in the Republic of Kazakhstan led to a general increase in both its yield and resistance to pathogenic microorganisms.

Keywords: adduct, fullerenol-24, transition metals, lanthanides, synthesis, identification, agricultural application, spring barley.

DOI: 10.61011/PSS.2023.12.57641.4932k

1. Introduction

To synthesize adducts of fullerenol-24 with transition metals and lanthanides, we used fullerenol-24 $C_{60}(OH)_{24}$ [1–9], which is interesting for its agrotechnical applications [10,11].

Synthesis of adducts $C_{60}(ONa)_x(O_2M)_{(24-x)/2}$, $C_{60}(ONa)_x(O_3M)_{(24-x)/3}$, M = Co, Cu, Mn, Zn, Gd, Tb were carried out in two stages. At the first stage, the synthesis of sodium derivatives of fullerenol took place, and at the second stage, the synthesis of adducts took place:

$$C_{60}(OH)_{24} + 24NaOH = C_{60}(ONa)_{24} + 24H_2O, \quad (1)$$

$$C_{60}(ONa)_{24} + [(24-x)/2]MCl_2 = C_{60}(ONa)_x(O_2M)_{(24-x)/2} + (24-x)NaCl, \quad (2)$$

$$C_{60}(ONa)_{24} + [(24-x)/3]MCl_3 = C_{60}(ONa)_x(O_3M)_{(24-x)/3} + (24-x)NaCl. \quad (3)$$

Equation (2) corresponds to the synthesis of adducts with transition metals, and equation (3) — with $4f$-metals (lanthanides).

The following methodology was used.

1. Dissolution of 2.9 g $C_{60}(OH)_{24}$ in 30 cm^3 of NaOH solution (solution concentration 0.1 mol/l), as a result of dissolution a brown aqueous solution $C_{60}(OHA)_{24}$ is formed. Bringing the solution pH to 7.5–8.5 rel. units by adding a few drops of HCl solution with a concentration of 1 mol/l.

2. Preparation of 100 ml of MCl_x (M = Co,Cu, Mn, Zn, Gd, Tb) solution with a concentration of 55 g/dm^3 ($CoCl_2$) up to 93 g/dm^3 ($TbCl_3$) at solution pH 3.5–4.0 rel. units to avoid hydrolysis of MCl_x (when adding a few drops of HCl solution with concentration of 1 mol/l).

3. Addition of aqueous solution MCl_x dropwise to aqueous solution $C_{60}(OHA)_{24}$. A loose amorphous colored precipitate is formed. Settling of the resulting solution with the precipitate formed for 24 h. Filtration of the resulting heterogeneous mixture (solution-solid phase) through a paper filter („red tape").

4. Washing three times of the precipitate with methanol CH_3OH, (for each washing $\sim$ 50 cm^3 of solvent was used). Final drying of the adducts in vacuum drying cabinet (residual pressure did not exceed 0.1 mm Hg) at temperature of $\sim$ 50°C for 90 min.

As a result, quantities in grams of colored crystalline hydrate adducts were obtained: $C_{60}(ONa)_{12}(O_2Co)_6 \cdot 24H_2O$, $C_{60}(ONa)_4(O_2Cu)_{10} \cdot 18H_2O$, $C_{60}(ONa)_4(O_2Mn)_{10} \cdot 18H_2O$, $C_{60}(ONa)_8(O_2Zn)_8 \cdot 20H_2O$, $C_{60}(ONa)_6(O_3Gd)_6 \cdot 22H_2O$, $C_{60}(ONa)_6(O_3Tb)_6 \cdot 20H_2O$ with weight of 3.8 g. (for $C_{60}(ONa)_{12}(O_2Co)_6 \cdot 24H_2O$) to 4.1 g (for $C_{60}(ONa)_6(O_3Gd)_6 \cdot 22H_2O$), which corresponds to the practical yield $\eta \approx 65-72\%$ of theoretically possible. Typical photographs of the synthesized adducts (presented in Figure 1) were taken on VEGA3 TESCAN electron microscope at magnification $\times 500-5000$.

Formation of adducts of $C_{60}(ONa)_x(O_2M)_{(24-x)/2}$, $C_{60}(ONa)_x(O_3M)_{(24-x)/3}$ type in acidic solutions was not

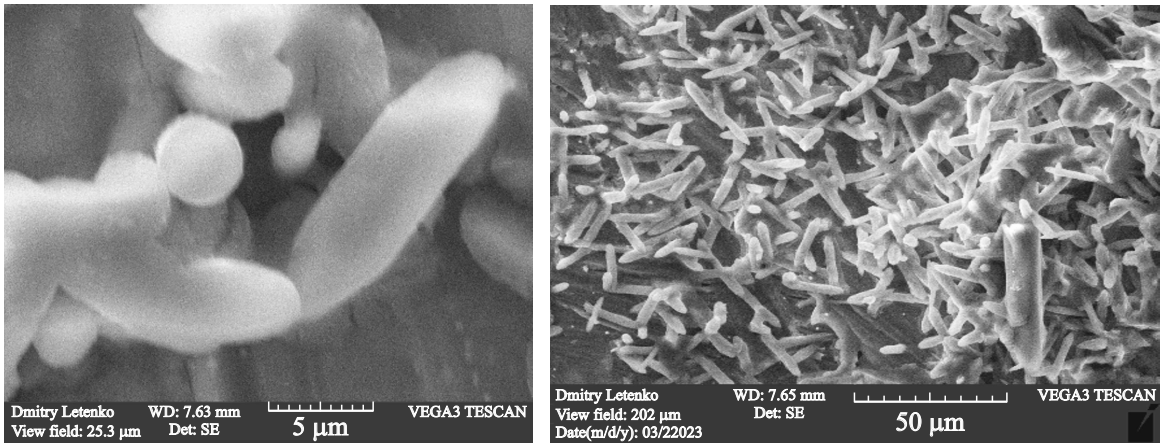

Figure 1. Electronic photographs of crystalline hydrates of adducts of fullerenol-24 with transition metals and lanthanides: *a* — $C_{60}(ONa)_4(O_2Mn)_{10} \cdot 18H_2O$ (magnification $\times 5000$), *b* — $C_{60}(ONa)_6(O_3Gd)_6 \cdot 22H_2O$ (magnification $\times 500$).

Table 1. Elemental composition of metal adducts of $C_{60}(ONa)_x(O_2M)_{(24-x)/2}$, $C_{60}(ONa)_x(O_3M)_{(24-x)/3}$

№	*M* in adduct	Element content per 1 molecule of fullerene core C_{60} (60 atoms C)					Formula of metal adduct
		C	O	H	Na	*Me*	
1	Na	60	44 ± 2	40 ± 2	24 ± 1	0	$C_{60}(OHA)_{24} \cdot 20H_2O$
2	Co	60	48 ± 6	48 ± 5	12 ± 3	6 ± 2	$C_{60}(ONa)_{12}(O_2Co)_6 \cdot 24H_2O$
3	Cu	60	42 ± 8	36 ± 5	4 ± 2	10 ± 4	$C_{60}(ONa)_4(O_2Cu)_{10} \cdot 18H_2O$
4	Mn	60	42 ± 9	36 ± 4	4 ± 2	10 ± 5	$C_{60}(ONa)_4(O_2Mn)_{10} \cdot 18H_2O$
5	Zn	60	44 ± 7	40 ± 5	8 ± 3	8 ± 3	$C_{60}(ONa)_8(O_2Zn)_8 \cdot 20H_2O$
6	Gd	60	46 ± 8	44 ± 6	6 ± 3	6 ± 3	$C_{60}(ONa)_6(O_3Gd)_6 \cdot 22H_2O$
7	Tb	60	44 ± 8	40 ± 7	6 ± 3	6 ± 3	$C_{60}(ONa)_6(O_2Tb)_6 \cdot 20H_2O$

observed in principle, which is clearly proven by analyzing solubility diagrams in ternary systems with fullerenol and a metal salt (fullerenol–metal salt–water) [1,2,12].

The adducts $C_{60}(ONa)_x(O_2M)_{(24-x)/2}$, $C_{60}(ONa)_x(O_3M)_{(24-x)/3}$, $M =$ Co, Cu, Mn, Zn, Gd, Tb were identified by the following methods. IR spectra of adducts in KBr tablets were obtained on Shimadzu FTIR-8400S spectrometer in the wavenumber range $\bar{\nu} = 400-4000\,\mathrm{cm}^{-1}$. Electronic absorption spectra were obtained on SPECORD M32 spectrophotometer (Germany) in the wavelength range $\lambda = 200-1000\,\mathrm{nm}$ (reference solution — distilled water). Thermogravimetric analysis of adducts was carried out on NETZSCH TG 209 F1 Libra analyzer in the temperature range $30-100^\circ$C in an air atmosphere with a heating rate of $5\,\mathrm{K} \cdot \mathrm{min}^{-1}$. For high performance liquid chromatography, we used Shimadzu LC-20 Prominence with spectrophotometric detection at $\lambda = 300\,\mathrm{nm}$, equipped with a column „Phenomenex® NH2“ (column with dimensions $150 \times 2.0\,\mathrm{mm}$, $5\,\mu\mathrm{m}$ and current 100 A), injection volume $2 \cdot 10^{-8}\,\mathrm{m}^3$, injection speed $0.2\,\mathrm{ml} \cdot \mathrm{min}^{-1}$, eluent — acetonitrile / aqueous solution of acetic acid with acid concentration 0.1% (in a volume ratio sample/solvent 5/95). The elemental composition was analyzed by X-ray fluorescence analysis using VEGA3 TESCAN scanning electron microscope with Essence software. Additionally, elemental analysis for the content of light atoms was carried out using PerkinElmer PE 2400 CHN device. Dynamic light scattering in aqueous solutions of adducts was carried out using Zetasizer Nano ZS device. The solubility of adducts in aqueous solutions was studied using a standard shaker-thermostat with additional temperature stabilization ($\Delta T = 0.05\,\mathrm{K}$, saturation time — 8 h, shaking frequency $\nu = 2\,\mathrm{Hz}$, the concentrations of solutions were determined by the spectrophotometric method at the wavelength $\lambda = 270\,\mathrm{nm}$).

The composition of the precursor $C_{60}(OHA)_{24} \cdot 20H_2O$ is established quite accurately ($\pm$1atom H, Na, O on 1 fullerene core — 60 atoms C, see Table 1). Some scattering in the O and H content is associated with the presence in all adducts of a large amount of weakly bound crystallization water, while on the surface of crystalline hydrates (when studied in the atmosphere), partial dehydration of equilibrium crystalline hydrates can occur. For metal adducts with transition metals and lanthanides *M* the stability of the composition is significantly reduced, first of all, this relates to the content of *M* in the adducts ($\pm 2-5$ atoms *M* per 60 atoms of C, Table 1). All adducts

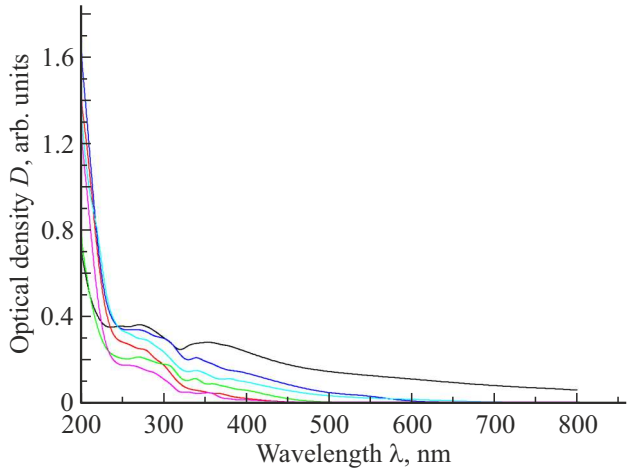

Figure 2. Electronic spectra of metal adducts of fullerenol-24 $C_{60}(ONa)_x(O_2M)_{(24-x)/2}$and $C_{60}(ONa)_x(O_3M)_{(24-x)/3}$relative to distilled water; M: Co (black), Cu (red), Mn (cyan), Zn (blue), Gd (green), Tb (purple); cuvette width $l = 10$ cm; concentrations of solutions in g/dm^3: Co — 0.040, Cu — 0.043, Mn — 0.040, Zn — 0.043, Gd — 0.037, Tb — 0.040.

can be considered mixtures of forms with slightly different compositions (related compounds) and their isomers. Primary precursors used for the preparation of adducts, namely $C_{60}(OH)_{24}$, $C_{60}Br_{24}$ [3,4], are a mixture of isomers, not always of a strictly stoichiometric composition. A halogen atom can be implanted to a pentagon-hexagonal C atom or to a hexagon-hexagonal C atom (then the structure will be inherited by fullerenol, its sodium forms and metal adducts). Further, substitution groups can alternatively be located evenly distributed over the surface of the core C_{60}, mainly along the equator of the core, circumferentially, by spots, etc. Already during the formation of metal adducts with two and three charged cations, binding is possible with groups of one fullerene core C_{60}, two or even three different cores. The average distance between adjacent substitution groups (C–O–Na) in the adduct $C_{60}(OHA)_{24}$can be calculated in the simplest way approximation of uniform distribution of groups over the surface of the core C_{60}: $r = (\pi d^2/N)^{1/2}$, where $d \sim 0.73$ nm — „diameter of fullerene core“, $N = 24$. The calculation yields the value $r \sim 0.26$ nm. Approximate bond length is $r_{C-O-Na} \approx 0.3-0.4$ nm. Taking into account the ionic radii M^{z+} (from $r_{M^{z+}} \approx 0.073$ for Cu to $r_{M^{z+}} \approx 0.092$ for Tb), geometrically, the binding of one multicharged ion can occur with either one or several fullerene cores.

From Figure 2 it is clear that the electronic spectra of solutions of all metal adducts are isomorphic: there are two broad absorption peaks at $\lambda_1 \sim 340-360$ nm, $\lambda_2 \sim 265-275$ nm. Based on the second peak, we subsequently determined the volume concentrations of adducts. Extinction coefficients ε_{270} for solutions of metal adducts at $\lambda = 270$ nm are presented in Table 2.

Table 2. Extinction coefficients ε_{270} and concentration c alculation coefficients $\varkappa_{270}$ for solutions of metal adducts at $\lambda = 270$ nm

M In metal adduct	Extinction coefficient ε_{270}, 10^3 cm^2/g	Concentration calculation coefficient $\varkappa_{270}$, g/dm^3
Co	0.915	1.093
Cu	0.572	1.748
Mn	0.850	1.176
Zn	0.391	2.557
Gd	0.568	1.760
Tb	0.733	1.364

The concentration of metal adducts C relates to the optical density D_{270} at $\lambda = 270$ nm (according to the Bouguer–Lambert–Beer law) by the relation

$$D_{270} = \varepsilon_{270} C(\text{g/dm}^3) l(\text{cm}),$$

$$C(\text{g/dm}^3) = D_{270}/\varepsilon_{270} l(\text{cm}) = \varkappa_{270} D_{270}/l, \qquad (4)$$

where $\varkappa_{270}$ — concentration calculation coefficient at $\lambda = 270$ nm according to the Bouguer–Lambert–Beer law.

The difference in extinction coefficients in the electronic spectra of aqueous solutions of metal-adducts by 2–3 times is associated, in the opinion of the authors, with fixing for convenience the wavelength of the spectrophotometric determination of volumetric concentrations of metal-adducts — $\lambda = 270$ nm, in which case the absorption maxima can shift by several nm or several tens of nm.

The IR absorption spectra of all metal adducts also turned out to be isomorphic. All represent: vibrations of the fullerene core C_{60} at values of wave number $\bar{\nu}$ in the intervals 528–532, 570–577, 1170–1183, 1423–1429 cm^{-1}; vibrations of crystalline hydrate molecules H_2O in the wave number ranges 3595–3620, 3448–3454, 1640–1651 cm^{-1}; relatively weak vibrations of residual and hydrolyzed O–H groups in the range of values $\bar{\nu} = 3417-3421$ cm^{-1}; vibrations of C–O groups in the range of values $\bar{\nu} = 1716-1728$ cm^{-1}; vibrations of O–Na groups at $\bar{\nu} = 540-565$ cm^{-1}; system of peaks corresponding to vibrations of M–O, O–M–O, in the range of values $\bar{\nu}$ from 424 cm^{-1} (Zn) up to 600 cm^{-1} (Tb).

A comprehensive thermal analysis of crystalline hydrates was carried out for crystalline hydrates of metal adducts $C_{60}(ONa)_x(O_2M)_{(24-x)/2} \cdot NH_2O$, $C_{60}(ONa)_x(O_3M')_{(24-x)/3} \cdot N'H_2O$, ($M$ = Co, Cu, Mn, Zn, M' = Gd, Tb). Let us denote $T^{(\text{start})}$, $T^{(\text{ext})}$, $T^{(\text{fin})}$ the temperatures of the beginning, extremum and end of the effect. Let us introduce the notation for the following processes: MED — multi-stage dehydration of crystalline hydrates, T–RE–OMD — decomposition with oxide release M, SOD — decomposition with release of oxide Na_2O, FCO — fullerene core additional oxidation.

In all cases, the corresponding effects were consistently observed in the thermograms. In MED process $T^{(\text{start})}$

Table 3. Size distribution of δ_i adduct associates in solutions at 25°C

Metal adduct	Concentration C, g/dm^3	δ_0, nm	δ_{I}, nm	δ_{II}, nm	δ_{III}, nm
$C_{60}(ONa)_{12}(O_2Co)_6$	0.34	–	65	105	7
$C_{60}(ONa)_4(O_2Cu)_{10}$	0.55	–	–	105	5
$C_{60}(ONa)_4(O_2Mn)_{10}$	0.49	–	–	108	5
$C_{60}(ONa)_8(O_2Zn)_8$	0.88	–	–	120	5
$C_{60}(ONa)_6(O_3Gd)_6$	0.72	–	–	120	6
$C_{60}(ONa)_6(O_2Tb)_6$	0.50	–	65	103	7

Table 4. Electrokinetic potentials ξ_i and mobility U_i of adduct associates in solutions at 25°C

Metal adduct	ξ_{I}, mV	ξ_{II}, mV	ξ_{III}, mV	U_{I}, μm · cm/V · s	U_{II}, μm · cm/V · s	U_{III}, μm · cm/V · s
$C_{60}(ONa)_{12}(O_2Co)_6$	−20	−35	−60	−1.4	−2.6	−3.5
$C_{60}(ONa)_4(O_2Cu)_{10}$	–	−35	−50	–	−2.6	−3.7
$C_{60}(ONa)_4(O_2Mn)_{10}$	–	−35	−50	–	−2.5	−3.7
$C_{60}(ONa)_8(O_2Zn)_8$	–	−40	−50	–	−2.3	−3.7
$C_{60}(ONa)_6(O_3Gd)_6$	–	−40	−55	–	−2.4	−3.6
$C_{60}(ONa)_6(O_2Tb)_6$	−20	−30	−60	−1.5	−2.8	−3.5

lies in the range from 70 K (for Cu) to 95 K (for Zn); $T^{(\text{ext})}$ — from 285 K (for Cu) to 325 K (for Tb); $T^{(\text{fin})}$ — from 330 K (for Cu) to 370 K (for Tb). In the process T–RE–OMD $T^{(\text{start})}$ is in the range from 330 K (for Cu) to 385 K (for Gd); $T^{(\text{ext})}$ — from 390 K (for Cu) to 470 K (for Tb); $T^{(\text{fin})}$ — from 485 K (for Cu) to 540 K (for Tb). During SOD process $T^{(\text{start})}$ varies in the range from 490 K (for Cu) to 545 K (for Tb); $T^{(\text{ext})}$ — from 565 K (for Cu) to 615 K (for Tb); $T^{(\text{fin})}$ — from 640 K (for Cu) to 685 K (for Tb). In the case of FCO, for all metal adducts it is impossible to determine $T^{(\text{start})} = 680$ K, $T^{(\text{ext})} = 1000$ K, $T^{(\text{fin})}$, the process is extended over indefinite temperature range.

The metal adducts were identified also using high performance liquid chromatography (HPLC). The conditions for chromatographic analysis were as follows: column „Phenomenex® NH2“ (column parameters — 150 × 2 mm, 5 μm, 100 A), eluent — acetonitrile / aqueous solution of trifluoroacetic acid with a concentration of 0.1% (in volume ratio of 5 : 95), elution rate $v = 0.2$ ml/min, volume of dosed sample — 20 μl, a diode matrix was used for detection. The results obtained, for example, for the metal adduct $C_{60}(ONa)_8(O_2Zn)_8$showed that when the adduct leaves column, a rather narrow output peak is observed (with a width at half maximum $\delta_{1/2} \leq 20$ s, which indirectly proves the production of a fairly pure adduct with a purity of 96–97 rel. wt.%). Similar data were obtained for other metal adducts.

Solubility in systems $C_{60}(ONa)_x(O_2M)_{(24-x)/2}$–$H_2O$, $C_{60}(ONa)_x(O_3M)_{(24-x)/3}$–$H_2O$ is shown in Figure 3. From Figure 3 it is clear that the solubility of all metal adducts (without changing the type of crystalline hydrate) increases with temperature decreasing, which is very valuable in agrotechnical terms, since the maximum supply of plants with microelements will be observed precisely at temperatures about 0°C (when the first snow melts or falls in the spring-autumn period), when demand in these elements is maximum for the development of grain crops. It is interesting to note that the solubility of the crystal solvate of the precursor $C_{60}\cdot 2Ar$ (Ar — benzene, toluene, o-xylene, o-dichlorobenzene . . .) increases with temperature increasing, and the solubility of unsolvated C_{60}, on the contrary, decreases monotonically with temperature increasing.

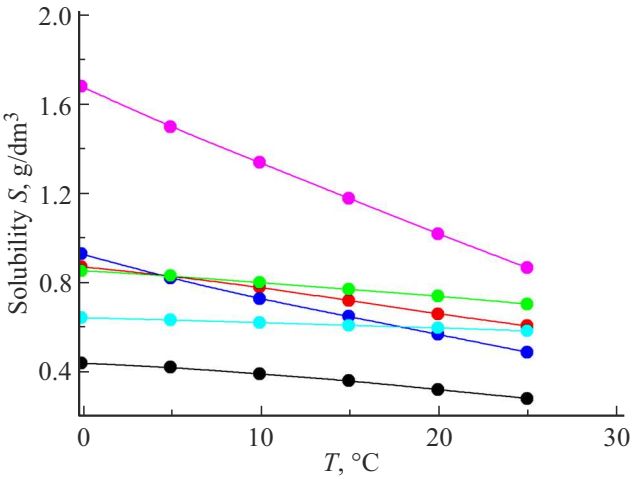

Figure 3. Solubility of metal adducts in water in the natural temperature range: Co (black), Cu (red), Mn (blue), Zn (blue), Gd (green), Tb (violet).

All solutions of metal adducts in water turned out to be hierarchically associated in a complex way (Tables 3, 4). In them the sequential formation of associates of I order are observed (with typical linear dimensions δ_{I} about tens nm), of II order (δ_{II} about hundreds nm), III order (δ_{III} about several microns), and the formation of the latter corresponds

to a microheterogeneous solution. unassociated metal adducts ($\delta_0 \sim 2\,\text{nm}$). Data on the distribution of metal adducts by size, electrokinetic potentials and mobility of adduct associates in solutions are presented in Tables 3, 4.

Elementary calculation of the number of monomer molecules in the associate of i-th order N_{i-0}

$$N_{i-0} = (\delta_i/\delta_0)^3 \cdot (K_{\text{pack}})^i, \; K_{\text{pack}} = \pi/6 \qquad (5)$$

allows you to estimate the required quantities: $N_{\text{I}-0} \approx 2 \cdot 10^4$, $N_{\text{II}-0} \approx (3-4) \cdot 10^4$, $N_{\text{III}-0} \approx (2-4) \cdot 10^9$ (K_{pack} — packing coefficient of „small spheres into large sphere“). The latter associates undoubtedly correspond to the microheterogeneous colloidal state of the system.

The negative potential of all associates, on the one hand, determines the sedimentation stability of solutions, and on the other hand, prevents further enlargement of associates of the III order.

To determine the biological yield of grain crops, nanopreparations prepared on the basis of fullerenol-24 itself and *M*adducts with transition metals (Co, Cu, Zn, Mn) were used. The most pronounced effect of their influence was shown in dryland areas with root treatment with solutions of water-soluble fullerenes fullerenol adducts with copper, manganese, cobalt and zinc, where the yield of spring barley increased by 54–80%. At other sites, the yield increased by 25–50%. This confirms the results of our previous studies [11].

Compared to other compounds of transition and rare earth metals, these compounds:

– are low-soluble, i. e. will remain in the soil for a long time;

– increase solubility with temperature decreasing, i. e. during the spring-autumn period (spring-winter crops), which is especially important for plants;

– exist in solutions in the forms of associates of various types — monomers and associates of I, II, III orders, each of which can be absorbed by different plant cells according to a different mechanism and with different diffusion restrictions;

– metal atoms associated with the fullerene core have, according to the authors opinion, a certain synergistic effect on plant cells, since fullerenols, by themselves (without metals in the structure), for example, have a pronounced antioxidant, moisture-preserving, anti-stress, bactericidal, etc. influence on plant cells.

Funding

The study was supported by a grant from the Russian Science Foundation No. 23-23-00064, https://rscf.ru/project/23-23-00064/.

Conflict of interest

The authors declare that they have no conflict of interest.

References

[1] K.N. Semenov, N.A. Charykov, V.N. Postnov, V.V. Sharoiko, I.V. Murin. Uspekhi khimii, **85**, *1*, 38 (2016). (in Russian). DOI: https://doi.org/10.1070/RCR4489

[2] N.A. Charykov, V.A. Keskinov, K.A. Tsvetkov, A. Kanbar, K.N. Semenov, L.V. Gerasimova, Zh.K. Shaimardanov, B.K. Shaimardanova, N.A. Kulenova. Processes **9**, *2*, 349 (2021). https://doi.org/10.3390/pr9020349

[3] M. Silion, A. Dascalu, M. Pinteala, B.C. Simionescu, C. Ungurenasu. Beilstein J. Org. Chem. **9**, 1285 (2013). https://doi.org/10.3762/bjoc.9.145

[4] J. Li, A. Takeuchi, M. Ozawa, X. Li, K. Saigo, K. Kitazawa. J. Chem. Soc. Chem. Commun. **23**, 1784 (1993). DOI: 10.1039/C39930001784

[5] S.M. Mirkov, A.N. Djordjevic, N.L. Andric, S.A. Andric, T.S. Kostic, G.M. Bogdanovic, M.B. Vojinovic-Miloradov, R.Z. Kovacevic. Nitric Oxide **11**, *2*, 201 (2004). DOI: 10.1016/j.niox.2004.08.003.

[6] A. Arrais, E. Diana. Fuller. Nanotub. Carbon Nanostructures **11**, 35 (2003). DOI: 10.1081/FST-120018667

[7] M.S. Meier, J. Kiegiel. Org. Lett. **3**, *11*, 1717 (2001). http://dx.doi.org/10.1021/ol0159120

[8] K. Kokubo, K. Matsubayashi, H. Tategaki, H. Takada, T. Oshima. ACS Nano **2**, *2*, 327 (2008). DOI: 10.1021/nn700151z.

[9] L.Y. Chiang, L-Y. Wang, J.W. Swirczewski, S. Soled, S. Cameron. J. Org. Chem. **59**, *14*, 3960 (1994). DOI: 10.1021/jo00093a030

[10] G.G. Panova, E.V. Kanash, K.N. Semenov N.A. Charykov, Yu.V. Khomyakov, L.M. Anikina, A.M. Artemyeva, D.L. Kornyukhin, V.E. Vertebny, N.G. Sinyavina, O.R. Udalova, N.A. Kulenova, S.Yu. Blokhina. Sel'skokhoz. biologiya **53**, *1*, 38 (2018). (in Russian). DOI: 10.15389/agrobiology.2018.1.38rus

[11] G.G. Panova, I.N. Ktitorova, O.V. Skobeleva, N.G. Sinjavina, N.A. Charykov, K.N. Semenov. Plant Growth Regul. **79**, *3*, 309 (2016). DOI: 10.1007/s10725-015-0135-x

[12] K.N. Semenov, I.G. Kanterman, N.A. Charykov, V.A. Keskinov, N.A. Kulenova. Radiokhimiya **56**, *5*, 421 (2014). (in Russian). DOI: 10.1134/S106636221405007

Translated by I.Mazurov